ISSN: 1410-8917
Jurnal Kimia Sains & Aplikasi
e-ISSN: 2597-9914

Jurnal Kimia Sains dan Aplikasi 24 (3) (2021): 77–84

Jurnal Kimia Sains dan Aplikasi
Journal of Scientific and Applied Chemistry

Journal homepage: http://ejournal.undip.ac.id/index.php/ksa

Addition of calcined $Na_2B_4O_7$ on the synthesis of $Li_7La_3Zr_2O_{12}$

Imam Shofid Alaih [a,1,*], Sidiq Fathonah [a], Khoirina Dwi Nugrahaningtyas [a], Fitria Rahmawati [a,2,*]

[a] Research Group of Solid-State Chemistry & Catalysis, Chemistry Department, Faculty of Mathematics and Natural Sciences, Sebelas Maret University, Surakarta, Indonesia

* Corresponding author: (1) shofidal@student.uns.ac.id; (2) fitria@mipa.uns.ac.id

https://doi.org/10.14710/jksa.24.3.77-84

Article Info

Article history:

Received: 7th December 2020
Revised: 19th March 2021
Accepted: 22nd March 2021
Online: 31st March 2021

Keywords:
LLZO garnet; B-Al doping; zirconia; all-solid-state lithium battery

Abstract

$Li_7La_3Zr_2O_{12}$ (LLZO) is a garnet-type electrolyte for all-solid-state lithium-ion batteries (ASSB). It has good chemical and electrochemical stability against lithium and a relatively high ionic conductivity. However, the ionic conductivity needs to be further increased to provide a high specific capacity of the ASSB. Element doping into LLZO is an effort to increase molecular defect, known to enhance the conductivity. This research studied the effect of the $Na_2B_4O_7$ addition on the LLZO synthesis, producing LLZBO(A). The investigation aims to understand whether the sodium ions dope into the LLZO structure during synthesis, or it is only B ions to enter into the structure. Therefore, another synthesis with B_2O_3 of B precursor was conducted for comparison (LLZBO(B)). The precursors were mixed stoichiometrically by following the formula of $Li_{7-x}La_{3-x}Zr_{2-x}B_xNa_xO_{12}$ (LLZBO, x= 0.15; 0.20; 0.30). XRD analysis equipped with Le Bail refinement found that LLZBO(A) and LLZBO(B) mainly consist of cubic and tetragonal LLZO with a %mol of 69.06 – 69.84 %, and the main secondary phase is $La_2Zr_2O_7$. The surface morphology of LLZBO(A) and LLZBO(B) is almost similar to the irregular form of large aggregates. The particles become more dispersed when 0.3 %mol dopant was submitted. Impedance analysis found a high ionic conductivity of LLZBAO(A)0.3 1.042×10^{-3} Scm^{-1}.

1. Introduction

The rechargeable lithium-ion batteries are still essential for various electrical devices as an extensive energy storage system [1, 2, 3, 4, 5, 6]. However, recently all-solid-state solid lithium-ion batteries, ASSB, have been investigated more due to the high power, high energy, and long life cycles with non-flammable solid electrolyte [7, 8, 9]. Various types of solid electrolytes have been reported, such as lithium superionic conductor (LISICON) [10], perovskite-type [11], sodium superionic conductor (NASICON) [12], garnet-type [13], and so forth. $Li_7La_3Zr_2O_{12}$ (LLZO) is a garnet type electrolyte family reported as a promising candidate with chemical and electrochemical stability against lithium and relatively high ionic conductivity [14, 15]. LLZO can be crystallized in the cubic phase and tetragonal phase. At room temperature, the cubic phase's ionic conductivity is higher than that of the tetragonal phase [16]. Various elements such as Al [17], Ga [18], Ge [19], Nb [20], Ta [21], W [22], Sm [23], Mg [24], and Gd [25] have been doped to stabilize the cubic phase of LLZO and increase the ionic conductivity.

Boron, B, is within a similar group with Aluminium, Al with three valence electrons, which potentially replaces Zr^{4+} within the structure, providing a vacancy site of oxygen ion. The addition of Boron from B_2O_3 precursor has been reported to reduce sintering temperatures and time of sintering [26], which is usually 1200°C for 36 hours or even more [27]. Glass can effectively promote the process of sintering by forming a liquid phase at high temperatures [28]. It can also increase the maximum relative density and ionic conductivity values of 92.4% and 1.86 $\times 10^{-4}$ Scm^{-1} [26]. Many precursors have been used for B precursors, such as H_3BO_3 [29], Li_3BO_3 [28], and B_2O_3 [26].

Some researchers also investigated multi-dopants insertion, such as Al-Ta doped into LLZO [30] and Ga-Ba-Ta doped LLZO [31]. Al-Ta doping investigation found that some of Li^+ was replaced by Al^{3+} and Ta^{5+}, producing cation vacancies due to relatively positive charges when

the higher oxidation number atoms replaced the lower Li^+. The cation vacancy number increases when some of Ta^{5+} also replace Zr^{4+} producing $Li_{7-3x-y}Al_xLa_3Zr_{2-y}Ta_yO_{12}$ [30]. The cation vacancies were also investigated when Ga^{3+} was replacing Li^+ and Ta^{5+} replacing Zr^{4+} [31]. Meanwhile, Ba^{2+} replaces La^{3+}, increasing the Li^+ concentration in the framework, leading to an increase in Li-ion conductivity [31].

This research conducted Na-B doping into $Li_7La_3Zr_2O_{12}$ simultaneously by sodium tetraborate, $Na_2Ba_4O_7$ addition. Meanwhile, Na's possibility is melted and released during sintering due to a low melting point of 97.8°C and a boiling point of 889°C [32]. Moreover, $Na_2B_4O_7$ has a melting point of 743°C. Therefore, for comparison, a single B doping was conducted by submitting B_2O_3 into LLZO for comparison. Based on Al doping into LLZO, it is estimated that B^{3+} (0.27 Å) will replace Li^+ (0.74 Å) [24], and based on the investigation result, La^{3+} can be replaced by a lower oxidation number of Ba^{2+} [31]. Therefore, it is estimated that Na^+ may replace La^{3+} producing $Li_{7-x}B_xLa_{3-y}Na_yZr_{2-x}O_{12}$. However, the possibility of Na to release after high-temperature sintering of 900°C is high, and the remaining B^{3+} to enter into the host structure producing cation vacancies.

This research investigated a different precursor of Boron source, i.e., a calcined sodium tetraborate decahydrate ($Na_2B_4O_7$) and Boron Dioxide (B_2O_3). Borax or $N_2B_4O_7.10H_2O$ is an inexpensive precursor; therefore, if the result is similar to B_2O_3 doping into LLZO, it will reduce many mass-production costs. Product characterization was used to confirm the result, including crystal structure, phase content, surface morphology, and impedance.

2. Methodology

Zirconia used to synthesis $Li_7La_3Zr_2O_{12}$ was a caustic fusion result of zircon, $ZrSiO_4$, by crushed the zircon sand with NaOH underweight ratio of 1.3: 1, followed by heating at 800°C for two hours [33]. Further treatments were water leaching in which the powder was soaked within distilled water and was stirred for 30 minutes at 100°C before filtration. The water leaching was conducted twice, followed by acid leaching using 37 % HCl solution under 100°C heating and stirred until form a homogeneous yellowish dispersion. The dispersion was then filtered to separate the clear-yellow solution as the $ZrOCl_2$ solution (ZOC solution) from the remaining white precipitate. The ZOC solution was then added with ammonium solution to precipitate the $Zr(OH)_4$ [33]. The precipitate was then washed with distilled water to neutralize the pH, followed by heating in the oven at 150°C for 3 h and calcined at 800°C for 5 h [32].

The sodium tetraborate decahydrate, $Na_2B_4O_5(OH)_4{\cdot}10H_2O$ (Borax), was mashed with mortar then was heated at 80-120°C for 2 h. The results obtained were then further heated at 170-200°C for 2 h. The second stage was gradual calcination at 400-600°C with a heating rate of 50°C/min. The result was anhydrous $Na_2B_4O_7$ as expected by equation (1) in which gradual heating up to 550°C can change the $Na_2B_4O_5$ $(OH)_4$ into $Na_2B_4O_7$ [34]. The produced powder was then crushed and sifted into 120 mesh.

$$Na_2B_4O_5(OH)_4\,2.75H_2O_{(s)} \xrightarrow{75\text{ - }170^{o}C} Na_2B_4O_5(OH)_{4(s)} + 2.75H_2O_{(g)}$$

$$Na_2B_4O_5(OH)_{4(s)} \xrightarrow{70\text{ - }550^{o}C} Na_2B_4O_{7(s)} + 2H_2O_{(g)} \quad (1)$$

The calcined-$Na_2B_4O_7$ was then analyzed with PXRD (Rigaku *miniflex 600* Cu-ray) and SEM/EDX (JEOL-JSM-6510LV). The calcined-$Na_2B_4O_7$ was then mixed with the LLZO precursors, Li_2CO_3 (99%, Merck), La_2O_3 (95%, Aldrich), and ZrO_2 powder that was prepared previously. The mixture was under a mole ratio of 7:3:4 for Li_2CO_3, La_2O_3, and ZrO_2, respectively [35]. The Li_2CO_3 was provided a 10% excess to prevent Li loss during sintering. The calcined-$Na_2B_4O_7$ was then added into the mixture under a stoichiometric ratio to produce the $Li_{7-x}La_{3-x}Zr_{2-x}B_xO_{12}$ compound, with x = 0.15; 0.20; 0.30, in which the extra addition of 1.4 % was applied to prevent lack of B source due to evaporation during sintering. The mixture was crushed until homogenous with an agate mortar and then pressed under a 10 KPa hydraulic press to form a pellet. The pellet was then calcined at 850°C for four hours with a heating rate of 5°C/min. The calcined sample was then crushed and was dispersed in ethanol and ground in a ball mill for four hours at 400 rpm. After ball milling, the powder was extracted and then mashed and filtered with 120 mesh, pressed isostatically (10 KPa) to form pellets, and sintered using alumina crush at 900°C for 5 hours [36].

The produced powder was then analyzed by PXRD (Rigaku miniflex 600 Cu-ray) equipped with Le Bail refinement to investigate the phase inside and fit with a definite- crystal structure and cell parameters. The surface morphology of the powder was also investigated with SEM-EDX (JEOL-JSM-6510LV). Impedance measurement with LCR meter (EUCOL U-2826, frequency of 20 Hz-5 MHz) was conducted to understand the resistance of a material by extracting resistance value, R, from ZView (a software embedded within Corrtest CS-150) fitting by applying an R-C network model. The impedance measurement was conducted at room temperature RT, 40, 50, and 100°C. The conductivity value was calculated from resistance, R, as a fitted result of the impedance curve using equation (2).

$$\sigma = \frac{1}{R}\frac{l}{A} \quad (2)$$

3. Results and Discussion

To characterize the precursors before conducting synthesis, the zirconia powder prepared from $ZrSiO_4$ was analyzed with XRD at 2θ of 10°-80°, as described within Figure 1. The diffraction pattern shows that there are two phases of monoclinic and tetragonal. Peaks define the tetragonal structure are at 2θ of 30.35°; 35.31°; 50.38°; and 60.49°. Meanwhile, the monoclinic phase reveals at 2θ of 28.33° and 31.82° [37]. Compared with the standard monoclinic ICSD # 172161 and tetragonal ICSD # 93028 diffraction as depicted in Figure 1, it confirms the existence of both phases.

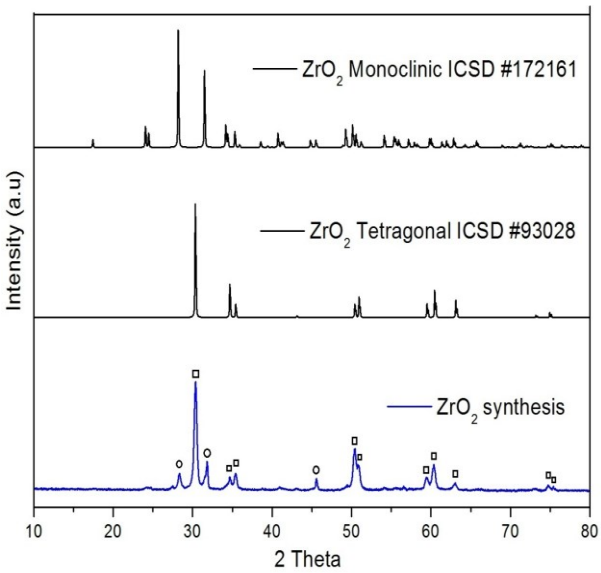

Figure 1. XRD patterns of ZrO_2 compare with the standard diffraction of tetragonal ZrO_2 ICSD#93028 and monoclinic ZrO_2 ICD#172161. The □ sign refers to tetragonal peaks, and the ○ sign refers to monoclinic peaks

The diffraction pattern of sodium tetraborate decahydrate ($Na_2B_4O_7.10H_2O$, Borax) and its calcination results are depicted in Figure 2. The highest peak of borax before calcination was at 2θ 31.51° and 34.92°. Meanwhile, after calcination at 600°C, two high peaks reveal at 2θ of 13.89° and 36.54° (Figure 2), which are matched well with the standard diffraction of $Na_2B_4O_7$ ICSD#2040. The other peaks reveal at the calcined-$Na_2B_4O_7$ also fit well with the characteristic peaks of the ICSD#2040. It seems that calcination successfully removes water molecules to be anhydrous $Na_2B_4O_7$. Even though sodium, Na will melt at 97.72°C [38], however, gradual heating until 600°C seems to did not remove Na and keep the core of sodium tetraborate to exist.

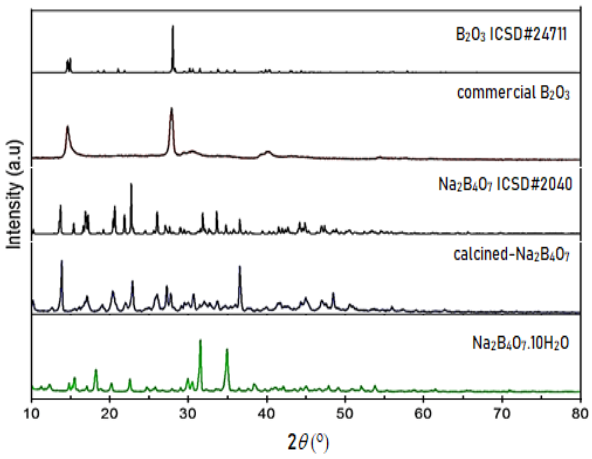

Figure 2. The XRD pattern of the initial sodium tetraborate decahydrate ($Na_2B_4O_7.10H_2O$) and its calcination results, compared with the standard $Na_2B_4O_7$ ICSD#2040 diffraction. The diffraction pattern of the commercial boron oxide (B_2O_3) and the B_2O_3 standard diffraction ICSD#24711

The Borax heating treatment follows some reaction stages in which at 170°C, about 17% or 3.5 moles of water content in borax was released gradually. On subsequent heating, i.e., 400-600°C, the bound water molecules were released. The release of H_2O molecules is explained in equation (3) [39].

$$Na_2B_4O_5(OH)_4{\cdot}8H_2O \xrightarrow{74^\circ C} Na_2B_4O_5(OH)_4{\cdot}4.5H_2O\ (3.5H_2O)\text{int.} \xrightarrow{120^\circ C}$$

$$Na_2B_4O_5(OH)_4{\cdot}4.5H_2O + 3.5H_2O\uparrow \xrightarrow{133^\circ C} Na_2B_4O_5(OH)_4{\cdot}3H_2O + 1.5H_2O$$

$$Na_2B_4O_5(OH)_4{\cdot}3H_2O \xrightarrow{133\text{-}200^\circ C} Na_2B_4O_5(OH)_{4(\text{amorph.})} + 3H_2O\uparrow \xrightarrow{200\text{-}500^\circ C}$$

$$[(Na_2B_4O_7)_{(\text{crystalline})}(Na_2B_4O_5)_{(\text{amorph})}] + 2H_2O\uparrow \xrightarrow{575^\circ C} Na_2B_4O_{7(\text{crystalline})} \quad (3)$$

At the beginning of heating, 3.5 moles of H_2O molecules were released at 120°C, then followed by releasing 1.5 moles H_2O at 133°C, and at 200°C $Na_2B_4O_5(OH)_4$ was amorphously formed by releasing 2 moles of H_2O. At 575°C, levels of H_2O in borax have been released to produce crystalline $Na_2B_4O_7$ [39]. Meanwhile, Boron has a melting and boiling temperature of 2075°C and 4000°C [32], respectively, which are very high. That ensures Boron, B stays after 600°C heating and receiving enough energy to dope into LLZO structure, whether through interstitial insertion or by replacing the lattice atoms to produce vacancies. Meanwhile, during heating at 950°C, sodium would be released by remaining boron oxide, B_2O_3, which melts and mixes with the LLZO precursor. To investigate whether B from the calcined-$Na_2B_4O_7$ able to diffuse into the LLZO structure during the LLZO formation, the calcined-$Na_2B_4O_7$ was mixed with LLZO precursors including Li_2CO_3, La_2O_3, and ZrO_2. For comparison, a commercial B_2O_3 was also mixed with the LLZO precursors. The mixture was stoichiometrically weighted based on the composition of x = 0.15, 0.2, and 0.3. The XRD patterns of the synthesis results are depicted in Figure 3 for the reaction of LLZO with $Na_2B_4O_7$. Meanwhile, the synthesis result of B_2O_3 with LLZO at various x produces diffraction patterns, as depicted in Figure 4.

Identical tetragonal LLZO peaks are in the range 2θ 25°-50°, and cubic LLZO characteristic peak is at 25.6°. Meanwhile, the LLZBO(A) in the variation of x = 0.15 0.2 shows peaks at 2θ 28.18° and 30.62°, which are considered typical peaks of tetragonal LLZO. Two peaks reveal at 2θ 28.84°, and 47.8° are indicating the presence of lanthanum zirconate. LLZBO(A) 0.15 and 0.2 moles have the same pattern at 2θ 15.9° and 31.8°, which correspond to the peaks of standard $Na_2B_4O_7$ #2040. Meanwhile, LLZBO (A) 0.3 has a peak at 20.6° according to $Na_2B_4O_7$ standard # 2040.

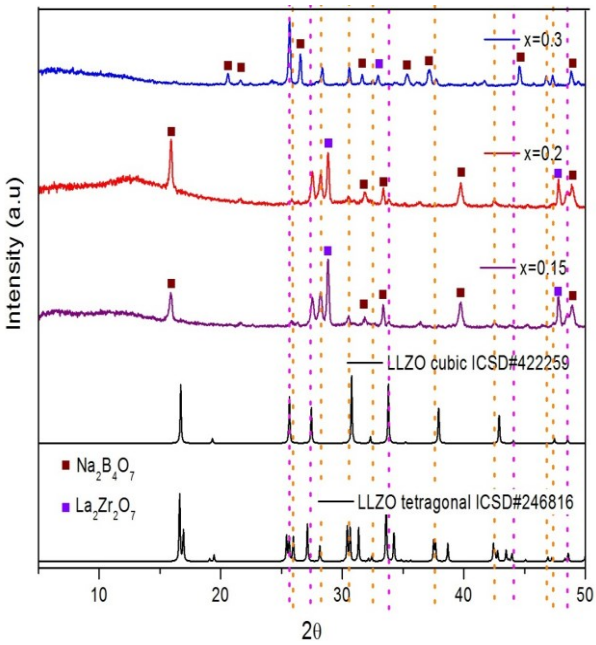

Figure 3. The XRD patterns of LLZBAO(A) at various x, compared with the standard diffraction of tetragonal LLZO ICSD#246816 and standard diffraction of cubic LLZO ICSD#422259

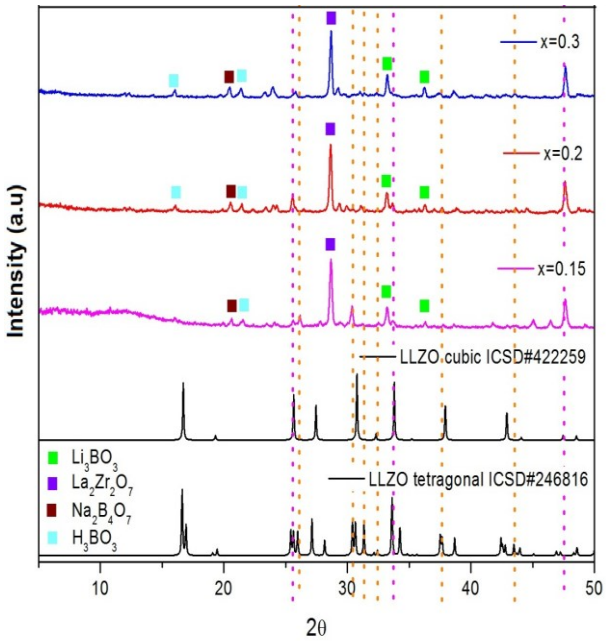

Figure 4. The XRD patterns of LLZBO(B) at various x compared with standard diffraction of tetragonal LLZO ICSD#246816 and standard diffraction of cubic LLZO ICSD#422259

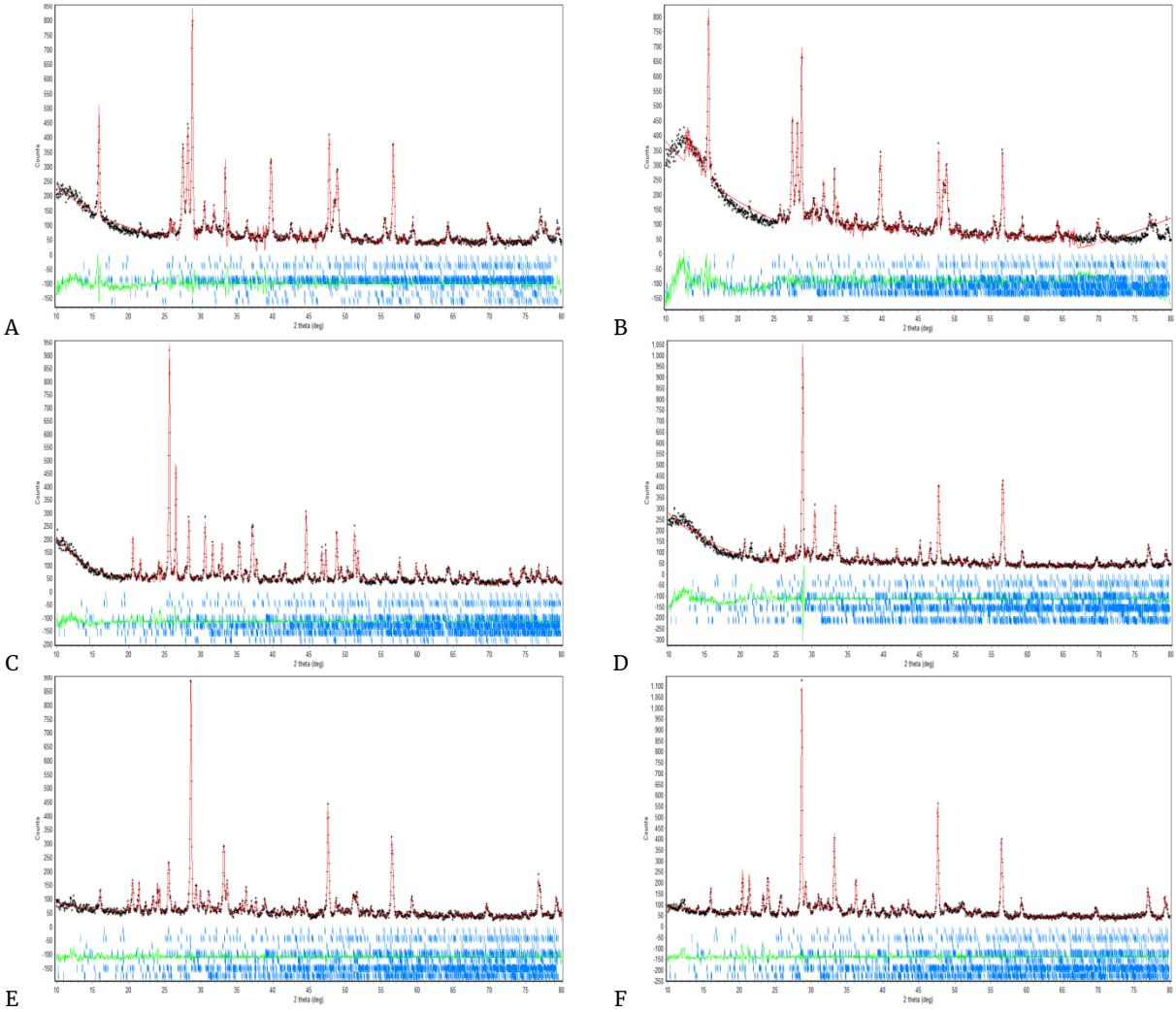

Figure 5. Le Bail plots of (a) LLZBO(A)0.15, (b) LLZBO(A)0.2, and (c)LLZBO(A)0.3, (d) LLZBO(B)0.15, (e) LLZBO(B)0.2, and (f) LLZBO(B) 0.3

Le Bail refinement was used to analyze further the phase content, crystal structure, and cell parameters. The Le Bail plots are depicted in Figure 5. Meanwhile, Table 1 provides phase composition in % mol as calculated by the refinement. The refinement shows that the main components of LLZBO(A) and LLZBO(B) are cubic and tetragonal LLZO, with % mol composition of 69.06 – 69.84 % consist of 34.49 ±0.11 % of cubic LLZO and 35.35±1.05 % of tetragonal LLZO for LLZBO(A). Meanwhile, LLZBO(B) consists of 34.19±0.53 % of cubic and 34.87±0.36 % of the tetragonal structure. The main secondary phase is $La_2Zr_2O_7$ with a composition of 20.163±0.025 %mol and 19.867±0.182 %mol for LLZBO(A) and LLZBO(B), respectively. The following secondary phase is H_3BO_3 at around 2%, as listed in Table 1. The rest are traces like lithium boron oxide and lithium zirconate and the remaining precursors. Cell parameters between LLZBO(A) and LLZBO(B) as calculated by Le Bail refinement are compared within Table 2 to estimate the elements that contribute to the solid-state reaction.

Table 1. Phase content within the prepared materials as resulted by Le Bail refinement

Phase	LLZBO(A)			LLZBO(B)		
	x=0.15	x=0.2	x=0.3	x=0.15	x=0.2	x=0.3
LLZO cubic	34.62	34.41	34.45	33.60	34.65	34.29
LLZO tetragonal	34.61	36.56	34.89	34.48	34.95	35.19
$La_2Zr_2O_7$ cubic	20.19	20.14	20.16	19.72	19.81	20.07
H_3BO_3 triclinic	2.16	2.22	2.15	2.12	2.14	2.10
Traces	8.42	6.66	8.35	10.09	8.42	8.25
Rp	6.72	10.72	8.03	8.58	7.05	7.11
Rwp	8.34	10.94	9.31	11.90	9.85	11.31

Table 2 shows that the cell parameter of cubic LLZBO(A) is greater than cubic LLZBAO(B) at about 0.0508 Å. It indicates different solid reactions due to Na ions in the synthesized mixture of LLZBO(A). The reaction is proposed in equation (4) according to the principle of Kroger-Vink notation for solid reaction.

$$Na_2B_4O_7 + Li_7La_3Zr_2O_{12} \rightarrow Li_{Li} + 2B_{Li}^{\bullet\bullet} + 4V_{Li}^{'} + La_{La} + 2Na_{La}^{''} + Zr_{Zr} + 2B_{Zr}^{'} + O_O + 3V_O^{\bullet\bullet} \quad (4)$$

Na insertion replacing La in its site producing 2- relative charge due to the different oxidation number of Na and La, which are 1+ and 3+, respectively. The production of 2- relative charge causes the formation of oxygen vacancies, $V_O^{\bullet\bullet}$. Meanwhile, if B_2O_3 only as a dopant, the reaction will produce only $0.5V_O^{\bullet\bullet}$ as depicted in equation (5).

$$B_2O_3 + Li_7La_3Zr_2O_{12} \rightarrow Li_{Li} + B_{Li}^{\bullet\bullet} + 2V_{Li}^{'} + LaLa + Zr_{Zr} + B_{Zr}^{'} + O_O + 0.5V_O^{\bullet\bullet} \quad (5)$$

Reaction (4) and (5) clearly show that the anion and cation vacancies can be formed more than when the dopant is B precursors only. The higher cell parameter of LLZBO(A) compares to LLZBO(B) supports the prediction by explaining that the anion vacancy, $V_O^{\bullet\bullet}$ bearing positive charge relative to the previous O^{2-} within site. The positive charge increases the bond length between atoms within the unit cell due to less electrostatic interaction than the interaction between O^{2-} with other cations in the LLZO structure. Meanwhile, the *a* and *b* side of tetragonal LLZBO(A) are lesser than the same side of LLZBO(B) due to when Na replace La ions, the long side will be reduced because the atomic radius of Na is 2.27 Å, which is less than the atomic radii of La, i.e., 2.43 Å [32].

Table 2. Cell parameters of cubic and tetragonal phases as calculated by Le Bail refinement by submitting cubic LLZO ICSD#422259 and tetragonal LLZO ICSD#246816

Cell parameters	LLZBO(A)		LLZBO(B)	
	Cubic structure ICSD#	Tetragonal structure ICSD#	Cubic structure ICSD#	Tetragonal structure ICSD#
a (Å)	13.0304	13.2740	12.9896	13.2971
b (Å)	13.0304	13.2740	12.9896	13.2971
c (Å)	13.0304	12.7189	12.9896	12.7186
α=β=γ	90	90	90	90
Rp (%)	8.03		7.11	
Rwp (%)	9.31		11.31	

The surface morphology of LLZBO(A) and LLZBO(B) are presented in Figure 6. LLZBO(A) and LLZBO(B) particle is similar to that of an irregular particle aggregated into a large particle of more than 10 μm diameter.

Figure 6 shows that the dopant composition of 0.3 mol produced more dispersed powder. LLZBO(A)0.3 more dispersed than LLZBO(B)0.3, even though the particle size of LLZBO(B) smaller, however the particle aggregates to form a larger particle. Small disperse particle size support higher surface area. This property, combined with more vacancies formed in LLZBO(A), as explained according to the refinement result (Table 2) and the proposed reactions (equation (4) and (5)), contributes to higher ionic conductivity of the LLZBO(A). The impedance plots are described in Figure 7, in which by increasing dopant composition into 0.3, the impedance was significantly decreased for both LLZBO(A) and LLZBO(B), allowing the ionic conductivity to increase up to 1.042×10^{-3} $Scm^{-1}$and 3.452×10^{-5} Scm^{-1}, for LLZBO(A) and LLZBO(B), respectively(Table 3). The abnormal grain growth, such as by aggregation, which occurred in LLZBO(B), as shown by Figure 6, causes the glassy phase can increase particle size and reduce its compactness, reducing its conductivity [26, 29]. Also, higher Li vacancies, $V_{Li}^{'}$ of LLZBO(A), as described in equation (4), is a significant parameter to explain the higher ionic conductivity of LLZBO(A) than the LLZBO(B). The number of oxygen vacancies in LLZBO(A) also larger than within LLZBO(B). The vacancies as a defect in a crystal structure have been known to significantly increase ionic conductivity due to defects, whether vacancies or interstitial defects are charge carriers within an ionic conductor [40].

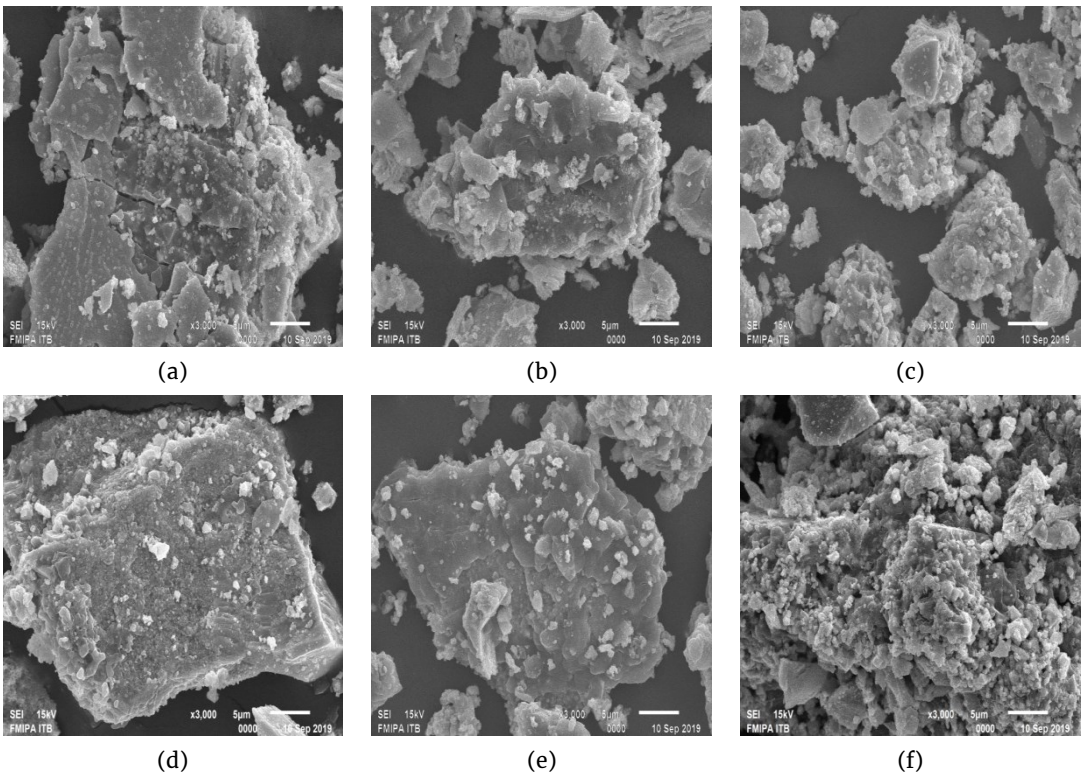

Figure 6. SEM images of (a) (a) LLZBO(A)0.15, (b) LLZBO(A)0.2, and (c)LLZBO(A)0.3, (d) LLZBO(B)0.15, (e) LLZBO(B)0.2, and (f) LLZBO(B) 0.3 under similar magnification

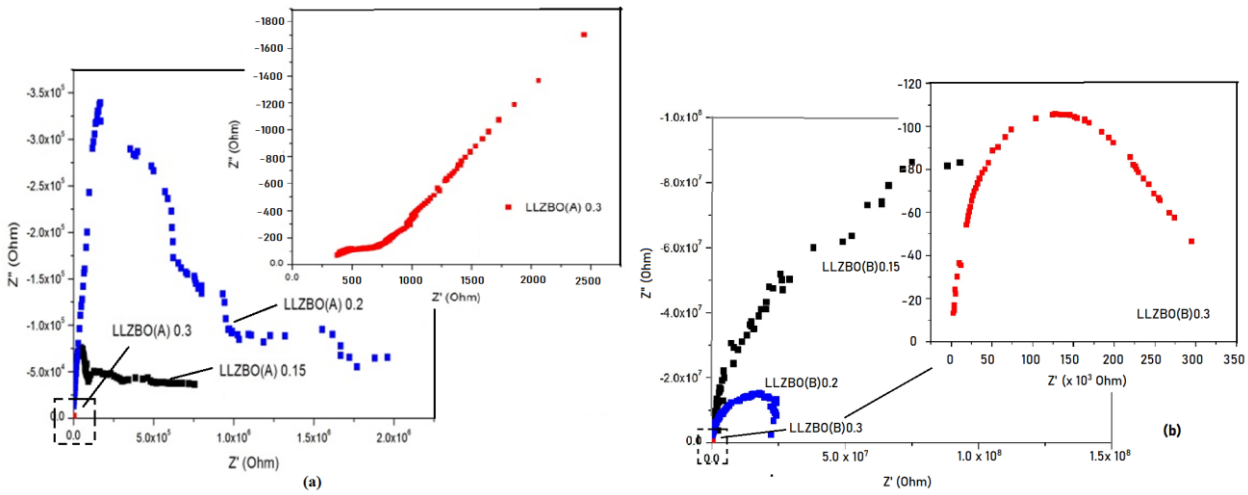

Figure 7. Nyquist plot (a) LLZBO(A) (b) LLZBO(B) at various compositions

Table 3. The ionic conductivity of LLZBO(A) and LLZBO(B)

X=	LLZBO (A)	LLZBO (B)
0.15	9.380×10^{-7}	2.980×10^{-9}
0.2	7.980×10^{-7}	2.061×10^{-8}
0.3	1.042×10^{-3}	3.452×10^{-5}

4. Conclusion

The addition of $Na_2B_4O_7$ into LLZO synthesis produced a material LLZBO(A) with phase composition dominated by cubic and tetragonal LLZO structure. The presence of Na ions affects the produced crystal. It was confirmed by Le Bail refinement in which the cell parameters of the cubic structure are higher than the cubic cell parameter of the material, which was prepared by B_2O_3 addition. It indicates the different cation and anion vacancies as predicted by solid-state reaction. The higher number of vacancies seems to contribute to the material's ionic conductivity, proven by the ionic conductivity value of LLZBO(A)0.3 1.042×10^{-3} Scm^{-1}, which is two orders higher than the ionic conductivity of LLZBO(B)0.3, i.e. 3.452×10^{-5} Scm^{-1}.

Acknowledgement

Authors acknowledge Universitas Sebelas Maret for providing research facilities related to this research, and also acknowledge Kemenristekdikti through PDUPT project for funding agreement of 2019/2020 and executed on 2021 due to pandemic situation.

References

[1] Zhenzhu Cao, Xueyan Cao, Xiaoting Liu, Weiyan He, Yanfang Gao, Jinrong Liu, Jiangtao Zeng, Effect of Sb-Ba codoping on the ionic conductivity of $Li_7La_3Zr_2O_{12}$ ceramic, *Ceramics International*, 41, 5, Part A, (2015), 6232-6236 https://doi.org/10.1016/j.ceramint.2015.01.030

[2] Kamil Burak Dermenci, Ahmet Furkan Buluç, Servet Turan, The effect of limonite addition on the performance of $Li_7La_3Zr_2O_{12}$, *Ceramics International*, 45, 17, Part A, (2019), 21401-21408 https://doi.org/10.1016/j.ceramint.2019.07.128

[3] Wenru Hou, Xianwei Guo, Xuyang Shen, Khali Amine, Haijun Yu, Jun Lu, Solid electrolytes and interfaces in all-solid-state sodium batteries: Progress and perspective, *Nano Energy*, 52, (2018), 279-291 https://doi.org/10.1016/j.nanoen.2018.07.036

[4] Minghui Hu, Yunxiao Li, Shuxian Li, Chunyun Fu, Datong Qin, Zonghua Li, Lithium-ion battery modeling and parameter identification based on fractional theory, *Energy*, 165, (2018), 153-163 https://doi.org/10.1016/j.energy.2018.09.101

[5] Junhao Li, Zhongqi Liu, Wen Ma, Hongying Dong, Kefu Zhang, Ruigang Wang, Low-temperature synthesis of cubic phase $Li_7La_3Zr_2O_{12}$ via sol-gel and ball milling induced phase transition, *Journal of Power Sources*, 412, (2019), 189-196 https://doi.org/10.1016/j.jpowsour.2018.11.040

[6] E. A. Il'ina, A. A. Raskovalov, A. P. Safronov, The standard enthalpy of formation of superionic solid electrolyte $Li_7La_3Zr_2O_{12}$, *Thermochimica Acta*, 657, (2017), 26-30 https://doi.org/10.1016/j.tca.2017.09.019

[7] Jun Ma, Bingbing Chen, Longlong Wang, Guanglei Cui, Progress and prospect on failure mechanisms of solid-state lithium batteries, *Journal of Power Sources*, 392, (2018), 94-115 https://doi.org/10.1016/j.jpowsour.2018.04.055

[8] Juliane Franciele Nonemacher, Claas Hüter, Hao Zheng, Jürgen Malzbender, Manja Krüger, Robert Spatschek, Martin Finsterbusch, Microstructure and properties investigation of garnet structured $Li_7La_3Zr_2O_{12}$ as electrolyte for all-solid-state batteries, *Solid State Ionics*, 321, (2018), 126-134 https://doi.org/10.1016/j.ssi.2018.04.016

[9] Chunwen Sun, Jin Liu, Yudong Gong, David P. Wilkinson, Jiujun Zhang, Recent advances in all-solid-state rechargeable lithium batteries, *Nano Energy*, 33, (2017), 363-386 https://doi.org/10.1016/j.nanoen.2017.01.028

[10] Audric Neveu, Vincent Pelé, Christian Jordy, Valerie Pralong, Exploration of Li–P–S–O composition for solid-state electrolyte materials discovery, *Journal of Power Sources*, 467, (2020), 228250 https://doi.org/10.1016/j.jpowsour.2020.228250

[11] Jiayao Lu, Ying Li, Yushi Ding, Structure, stability, and ionic conductivity of perovskite $Li_{2x-y}Sr_{1-x-y}La_yTiO_3$ solid electrolytes, *Ceramics International*, 46, 6, (2020), 7741-7747 https://doi.org/10.1016/j.ceramint.2019.11.277

[12] Sumaletha Narayanan, Samuel Reid, Shantel Butler, Venkataraman Thangadurai, Sintering temperature, excess sodium, and phosphorous dependencies on morphology and ionic conductivity of NASICON $Na_3Zr_2Si_2PO_{12}$, *Solid State Ionics*, 331, (2019), 22-29 https://doi.org/10.1016/j.ssi.2018.12.003

[13] Liwei Shen, Li Wang, Zhangjun Wang, Chao Jin, Lin Peng, Xiaowei Pan, Jiawen Sun, Ruizhi Yang, Preparation and characterization of Ga and Sr co-doped $Li_7La_3Zr_2O_{12}$ garnet-type solid electrolyte, *Solid State Ionics*, 339, (2019), 114992 https://doi.org/10.1016/j.ssi.2019.05.027

[14] Yali Luo, Yanli Zhang, Qixi Zhang, Yifeng Zheng, Han Chen, Lucun Guo, Effect of dual doping on the structure and performance of garnet-type $Li_7La_3Zr_2O_{12}$ ceramic electrolytes for solid-state lithium-ion batteries, *Ceramics International*, 45, 14, (2019), 17874-17883 https://doi.org/10.1016/j.ceramint.2019.06.002

[15] Jianli Gai, Erqing Zhao, Furui Ma, Deye Sun, Xiaodi Ma, Yongcheng Jin, Qingliu Wu, Yongjie Cui, Improving the Li-ion conductivity and air stability of cubic $Li_7La_3Zr_2O_{12}$ by the co-doping of Nb, Y on the Zr site, *Journal of the European Ceramic Society*, 38, 4, (2018), 1673-1678 https://doi.org/10.1016/j.jeurceramsoc.2017.12.002

[16] Chongyang Shao, Zhiyong Yu, Hanxing Liu, Zhenning Zheng, Nian Sun, Chunli Diao, Enhanced ionic conductivity of titanium doped $Li_7La_3Zr_2O_{12}$ solid electrolyte, *Electrochimica Acta*, 225, (2017), 345-349 https://doi.org/10.1016/j.electacta.2016.12.140

[17] Zhongli Hu, Hongdong Liu, Haibo Ruan, Rong Hu, Yongyao Su, Lei Zhang, High Li-ion conductivity of Al-doped $Li_7La_3Zr_2O_{12}$ synthesized by solid-state reaction, *Ceramics International*, 42, 10, (2016), 12156-12160 https://doi.org/10.1016/j.ceramint.2016.04.149

[18] Jianmeng Su, Xiao Huang, Zhen Song, Tongping Xiu, Michael E. Badding, Jun Jin, Zhaoyin Wen, Overcoming the abnormal grain growth in Ga-doped $Li_7La_3Zr_2O_{12}$ to enhance the electrochemical stability against Li metal, *Ceramics International*, 45, 12, (2019), 14991-14996 https://doi.org/10.1016/j.ceramint.2019.04.236

[19] R. H. Brugge, J. A. Kilner, A. Aguadero, Germanium as a donor dopant in garnet electrolytes, *Solid State Ionics*, 337, (2019), 154-160 https://doi.org/10.1016/j.ssi.2019.04.021

[20] Xiao Huang, Zhen Song, Tongping Xiu, Michael E. Badding, Zhaoyin Wen, Sintering, micro-structure and Li^+ conductivity of $Li_{7-x}La_3Zr_{2-x}Nb_xO_{12}$/MgO (x = 0.2–0.7) Li-Garnet composite ceramics, *Ceramics International*, 45, 1, (2019), 56-63 https://doi.org/10.1016/j.ceramint.2018.09.133

[21] Yu Gong, Zhan-Guo Liu, Yu-Jun Jin, Jia-Hu Ouyang, Lei Chen, Yu-Jin Wang, Effect of sintering process on the microstructure and ionic conductivity of $Li_{7-x}La_3Zr_{2-x}Ta_xO_{12}$ ceramics, *Ceramics International*, 45,

15, (2019), 18439-18444 https://doi.org/10.1016/j.ceramint.2019.06.061

[22] Yiqiu Li, Zheng Wang, Yang Cao, Fuming Du, Cheng Chen, Zhonghui Cui, Xiangxin Guo, W-Doped $Li_7La_3Zr_2O_{12}$ Ceramic Electrolytes for Solid State Li-ion Batteries, *Electrochimica Acta*, 180, (2015), 37-42 https://doi.org/10.1016/j.electacta.2015.08.046

[23] Xishu Wang, Jie Liu, Rui Yin, Yichen Xu, Yonghua Cui, Liang Zhao, Xibin Yu, High lithium ionic conductivity of garnet-type oxide $Li_{7+x}La_3Zr_{2-x}Sm_xO_{12}$ (x = 0–0.1) ceramics, *Materials Letters*, 231, (2018), 43-46 https://doi.org/10.1016/j.matlet.2018.08.006

[24] Amardeep, Sushobhan Kobi, Amartya Mukhopadhyay, Mg-doping towards enhancing the composition-phase-structural stability of Li-La-zirconate based cubic garnet upon exposure to air, *Scripta Materialia*, 162, (2019), 214-218 https://doi.org/10.1016/j.scriptamat.2018.11.026

[25] Shidong Song, Butian Chen, Yanli Ruan, Jian Sun, Limei Yu, Yan Wang, Joykumar Thokchom, Gd-doped $Li_7La_3Zr_2O_{12}$ garnet-type solid electrolytes for all-solid-state Li-Ion batteries, *Electrochimica Acta*, 270, (2018), 501-508 https://doi.org/10.1016/j.electacta.2018.03.101

[26] Yu Tang, Zhiwei Luo, Taoyong Liu, Piao Liu, Zhuo Li, Anxian Lu, Effects of B_2O_3 on microstructure and ionic conductivity of $Li_{6.5}La_3Zr_{1.5}Nb_{0.5}O_{12}$ solid electrolyte, *Ceramics International*, 43, 15, (2017), 11879-11884 https://doi.org/10.1016/j.ceramint.2017.06.035

[27] Ramaswamy Murugan, Venkataraman Thangadurai, Werner Weppner, Fast Lithium Ion Conduction in Garnet-Type $Li_7La_3Zr_2O_{12}$, *Angewandte Chemie International Edition*, 46, 41, (2007), 7778-7781 https://doi.org/10.1002/anie.200701144

[28] Ran-Hee Shin, Sam Ick Son, Yoon Soo Han, Young Do Kim, Hyung-Tae Kim, Sung-Soo Ryu, Wei Pan, Sintering behavior of garnet-type $Li_7La_3Zr_2O_{12}$-Li_3BO_3 composite solid electrolytes for all-solid-state lithium batteries, *Solid State Ionics*, 301, (2017), 10-14 https://doi.org/10.1016/j.ssi.2017.01.005

[29] E. A. Il'ina, S. V. Pershina, B. D. Antonov, A. A. Pankratov, E. G. Vovkotrub, The influence of the glass additive Li_2O-B_2O_3-SiO_2 on the phase composition, conductivity, and microstructure of the $Li_7La_3Zr_2O_{12}$, *Journal of Alloys and Compounds*, 765, (2018), 841-847 https://doi.org/10.1016/j.jallcom.2018.06.154

[30] Dong Ok Shin, Kyungbae Oh, Kwang Man Kim, Kyu-Young Park, Byungju Lee, Young-Gi Lee, Kisuk Kang, Synergistic multi-doping effects on the $Li_7La_3Zr_2O_{12}$ solid electrolyte for fast lithium ion conduction, *Scientific Reports*, 5, 1, (2015), 18053 https://doi.org/10.1038/srep18053

[31] Yedukondalu Meesala, Yu-Kai Liao, Anirudha Jena, Nai-Hsuan Yang, Wei Kong Pang, Shu-Fen Hu, Ho Chang, Chia-Erh Liu, Shih-Chieh Liao, Jin-Ming Chen, Xiangxin Guo, Ru-Shi Liu, An efficient multi-doping strategy to enhance Li-ion conductivity in the garnet-type solid electrolyte $Li_7La_3Zr_2O_{12}$, *Journal of Materials Chemistry A*, 7, 14, (2019), 8589-8601 https://doi.org/10.1039/C9TA00417C

[32] William M. Haynes, *CRC Handbook of Chemistry and Physics*, 97th ed., CRC Press, 2016

[33] Karima Apriany, Ita Permadani, Dani G. Syarif, Syoni Soepriyanto, Fitria Rahmawati, Electrical conductivity of zirconia and yttrium-doped zirconia from Indonesian local zircon as prospective material for fuel cells, *IOP Conference Series: Materials Science and Engineering*, 107, (2016), 012023 https://doi.org/10.1088/1757-899X/107/1/012023

[34] Ömer Şahin, A Nusret Bulutcu, Evaluation of Thermal Decomposition Kinetics of Borax Pentahydrate Using Genetic Algorithm Method by Isothermal Analysis, *Turkish Journal of Chemistry*, 27, 2, (2003), 197-208

[35] Junji Awaka, Norihito Kijima, Hiroshi Hayakawa, Junji Akimoto, Synthesis and structure analysis of tetragonal $Li_7La_3Zr_2O_{12}$ with the garnet-related type structure, *Journal of Solid State Chemistry*, 182, 8, (2009), 2046-2052 https://doi.org/10.1016/j.jssc.2009.05.020

[36] Liuliu Feng, Ling Li, Yunqiang Zhang, Hongjian Peng, Yingping Zou, Low temperature synthesis and ion conductivity of $Li_7La_3Zr_2O_{12}$ garnets for solid state Li ion batteries, *Solid State Ionics*, 310, (2017), 129-133 https://doi.org/10.1016/j.ssi.2017.08.016

[37] Beena Tyagi, Kalpesh Sidhpuria, Basha Shaik, Raksh Vir Jasra, Synthesis of Nanocrystalline Zirconia Using Sol-Gel and Precipitation Techniques, *Industrial & Engineering Chemistry Research*, 45, 25, (2006), 8643-8650 https://doi.org/10.1021/ie060519p

[38] Pradyot Patnaik, *Handbook of Inorganic Chemicals*, McGraw-Hill, 2003

[39] I. Waclawska, Thermal decomposition of borax, *Journal of thermal analysis*, 43, 1, (1995), 261-269 https://doi.org/10.1007/BF02635993

[40] Fitria Rahmawati, Bambang Prijamboedi, Syoni Soepriyanto, Ismunandar, SOFC composite electrolyte based on LSGM-8282 and zirconia or doped zirconia from zircon concentrate, *International Journal of Minerals, Metallurgy, and Materials*, 19, 9, (2012), 863-871 https://doi.org/10.1007/s12613-012-0640-0